Supporting Information

High-Performance Silicon Photoanode Enabled by Oxygen Vacancy Modulation on NiOOH Electrocatalyst for Water Oxidation

Qian Cai[a], Wenting Hong[a,b], Chuanyong Jian[a,b], Wei Liu*[a]

S1. The calculation of transient time constant (τ)

To quantitatively determine the charge recombination behavior, a normalized parameter (*D*) is introduced: $D = \frac{I_t - I_{st}}{I_{in} - I_{st}}\ (Equation\ S1)$, where I_t, I_{st} and I_{in} are the time-dependent, steady-state and initial photocurrent, respectively, as shown in **Fig. 4(e)**. The transient time constant (τ) is defined as the time when $lnD = -1$ in the normalized plots of $lnD \sim t$ as shown in **Fig. 4(f)**. The value of τ reflects the behavior of charge recombination and lifetime of the charge carriers.

S2. The calculation process of applied bias photon-to-current efficiency (ABPE)

The overall applied bias photon-to-current efficiency (ABPE, *%*) of the photoanode can be calculated from LSV data by the following equation: $ABPE\ (\%) = \frac{J_{mp}\left(E^{0}_{\frac{H_2O}{O_2}} - V_{app}\right)}{P_{in}} \times 100\%\ (Equation\ S2)$, where J_{mp} is the externally measured current density from LSV curves; V_{app} is the applied electrode bias; *E* is the Nernst potential for water oxidation (1.23 V); P_{in} is the incident optical power density (100 mW·cm^{-2}). The calculated ABPE values represent the upper limit of the conversion efficiency under the applied bias for a half cell.

S3. The incident-photon-to-current-efficiency (IPCE) measurements

IPCE was measured in a square quartz cell, using a Xenon lamp coupled with a monochromator as the light source under a CEL-SL-300 electrochemical testing system. The wavelength scan range is from 400 to 1000 nm and the photocurrent is obtained by subtracted the dark currents.

The incident-photon-to-current-efficiency (IPCE) as a function of wavelength for the prepared photoanodes was measured at a bias of 1.4 V versus RHE in 1.0 M KOH electrolyte. The IPCE was calculated by equation (S3):

$$\text{IPCE}\ (\%) = \frac{1240 \times J_{ph}}{P_{mono} \times \lambda} \times 100\% \qquad \text{(Equation S3)}$$

where J_{ph} is the photocurrent density (mA·cm^{-2}), P_{mono} is the intensity of the incident monochromatic light (mW·cm^{-2}), and λ is the wavelength of the monochromatic light.

S4. Flatband potential (E_{fb}) and barrier height (φ_{bh}) measurements

The flat band potential was measured in impedance potential mode on a CHI 660E station at 1 kHz in 1.0 M KOH solution electrolyte and keep in the dark during the measurements. The fluctuation voltage was set to 5 mV rms. A potential scan started from -0.6 V to 0.8 V versus Ag/AgCl. Operation frequency was 50 kHz. All measurements were conducted after 5 minutes open-circuit delay in a dark environment, the flat band potential was estimated by extrapolating linear region of the plot:

$$\frac{1}{C^2} = \frac{2}{A^2\varepsilon\varepsilon_0 q N_D}\left(E - E_{fb} - \frac{kT}{q}\right) \qquad (Equation\ S4\ )$$

C is the capacitance in the space charge layer, A is the area of photoanode exposed to electrolyte, ε is the relative permittivity of Si semiconductor (11.9), ε_0 is the vacuum permittivity (8.854×10^{-14} F/cm), q is the charge of an electron (1.60×10^{-19} C), N_D is the doping concentration, E is the difference between the applied potential and the redox potential of the solution, k is Boltzmann's constant (1.38×10^{-23}), and T is the temperature (298 K).

The doping density N_D was calculated using:

$$N_D = \frac{2}{A^2 q\varepsilon\varepsilon_0[\frac{d(\frac{1}{C^2})}{dV_{app}}]} \qquad (Equation\ S5)$$

The barrier height φ_b can be calculated by the following formulas:

$$\varphi_{hb} = V_{fb} + V_n \qquad \text{(Equation S6)}$$

$$V_n = kTln\frac{N_D}{N_C} \qquad (Equation\ S7)$$

N_C is the intrinsic doping density of Si (2.8×10^{19} cm^{-3}). The donor density (N_D) of the silicon wafer is calculated to be f8.3 x 10^{15} cm^{-3} rom Eq. where the charge of an electron as q (1.60 x 10^{-19} C), the electron mobility as μ (1500 cm^2 V^{-1} s-^{1}). The (100) n-silicon wafer used in this study had a resistivity (ρ) of 0.5 Ω·cm^{-1}.

$$N_D = \frac{1}{q\mu\rho} \ (Equation\ S8)$$

Finally, Vn is calculated to be 0.2 eV. And the values of barrier height of n-Si/Ni, n-Si/Ni/NiOOH and n-Si/Ni/NiOOH/NiFe photoanodes were calculated to be 0.93 eV, 0.97 eV and 1.01 eV, respectively.

Supplementary Figures

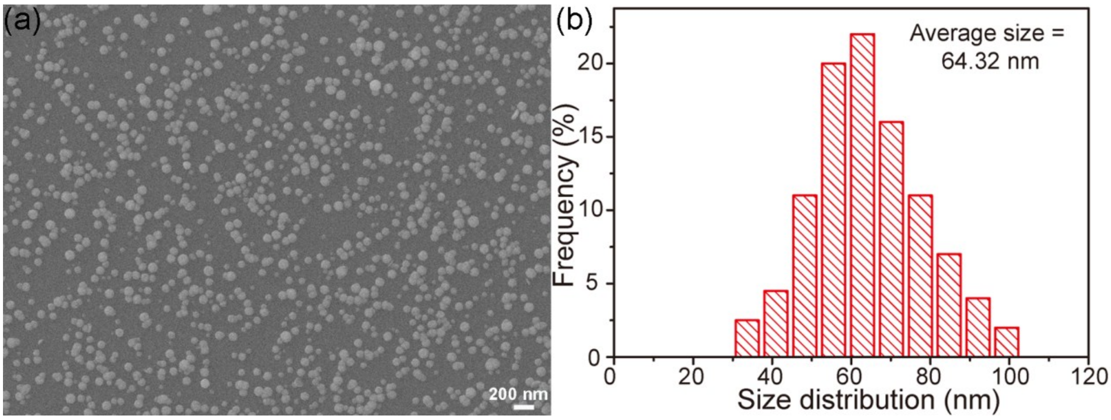

Fig. S1 Scanning electron microscope (SEM) image and the statistical size distribution histogram of n-Si/Ni/NiOOH/NiFe photoanode.

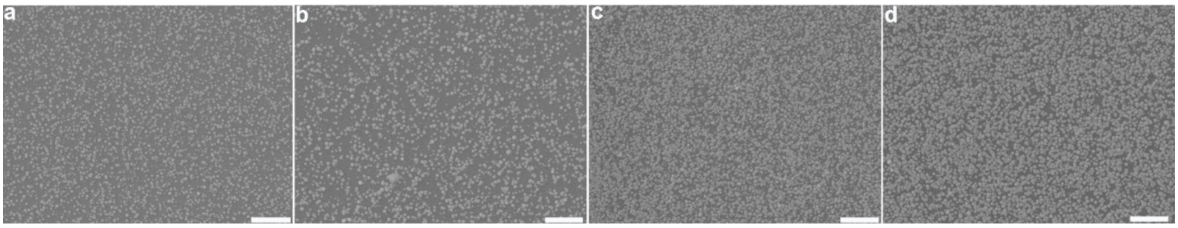

Fig. S2 SEM images of the prepared n-Si/Ni/NiOOH photoanodes with various Ni electrodeposition time at the potential of -1.5 V vs Ag/AgCl electrode: **(a)** 3s, **(b)** 5s, **(c)** 10s, **(d)** 15s. The sale bar is 1 μm.

The size and the surface coverage of the Ni nanoparticles on the Si photoanode allows convenient controlled by adjusting the electrodeposition time. SEM images demonstrated that as prolong the electrodeposition time, the size and the surface coverage of the Ni nanoparticles is obviously increasing.

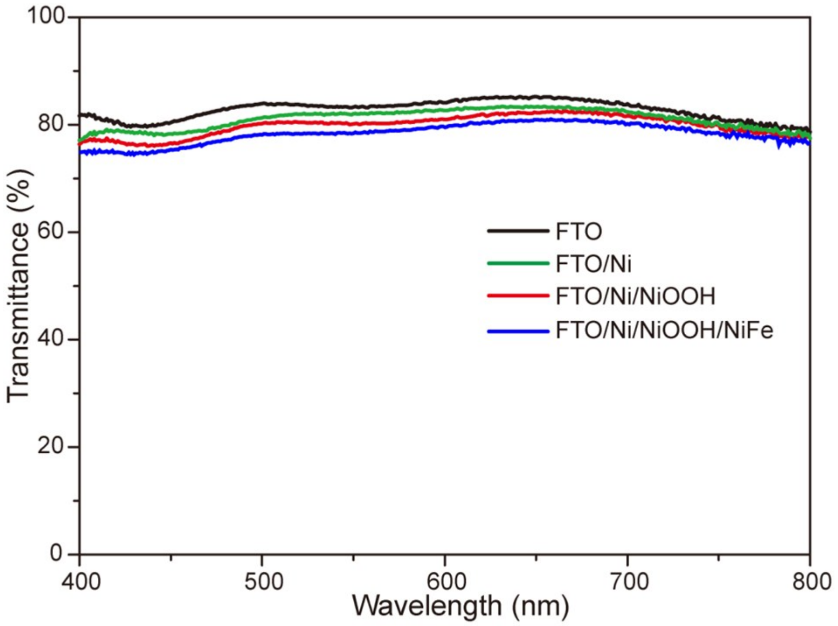

Fig. S3 Transmittance spectra of various Ni electrocatalysts on FTO glass substrate.

The optical transmittance measurements further demonstrate that the island-like Ni films only partially covering the substrate surface ensures sufficient light absorption for the photoelectrode, which will not significantly affect the light absorption of the Si substrate.

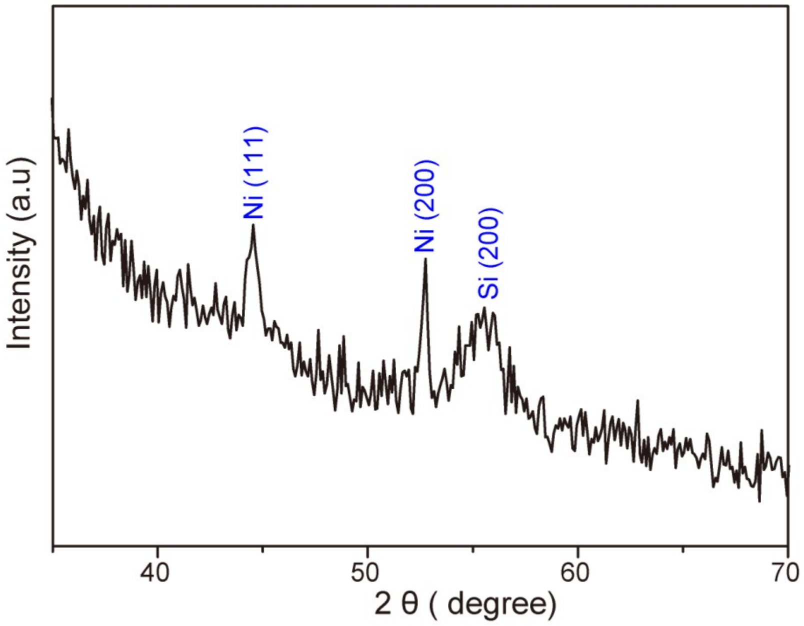

Fig. S4 GIXRD patterns of the prepared n-Si/Ni/NiOOH/NiFe photoanode.

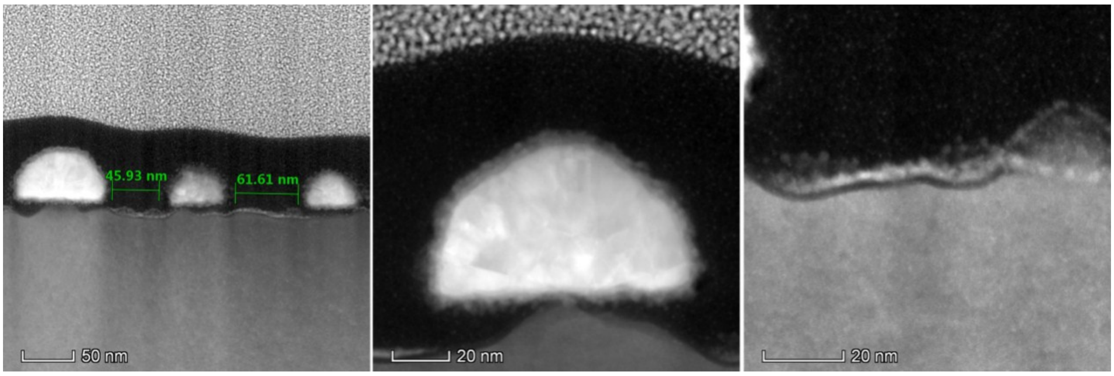

Fig. S5 HAADF-STEM images of the prepared n-Si/Ni/NiOOH/NiFe photoanode.

The HAADF-STEM images reveal that the bright spots corresponding to NiFe nanoparticles are uniformly anchored onto NiOOH and Si/SiO$_x$ surface. The uniformly anchored NiFe not only can maximize the exposure of the active sites, also can be employed as a protection layer to prevent Si photocorrosion.

Tab. S1 XPS results of different samples for Ni $_{2p}$ and O$_{1s}$ spectra.

Sample	**Ni^{3+} (Area)**	**Ni^{2+} (Area)**	**Area ratio Ni^{3+}/total Ni (%)**	**Atomic ratio (Ni^{3+}/Ni^{2+})**	**O$_v$ (Area)**	**Area ratio O$_v$/total O (%)**
NiOOH	8754.8	2940.8	64	2.98	5209.2	18.1
NiOOH/NiFe [(a)]	27800	5895.4	71.5	4.71	15240	40.6

NiOOH/NiFe **(b)**	27800	/	100	/	16430	43.6

(a) Before OER testing; **(b)** after OER testing

Tab. S2 The shifts of the Ni binding energies extract from XPS data.

Peak position	**Ni 2p$_{1/2}$**		**Ni 2p$_{3/2}$**	
	Ni^{2+}	Ni^{3+}	Ni^{2+}	Ni^{3+}
Positive shift (eV)	1.7	1.3	0.5	0.15

Both the Ni^{2+}or Ni^{3+} shows a positive shift to the higher binding energy after NiFe decoration.

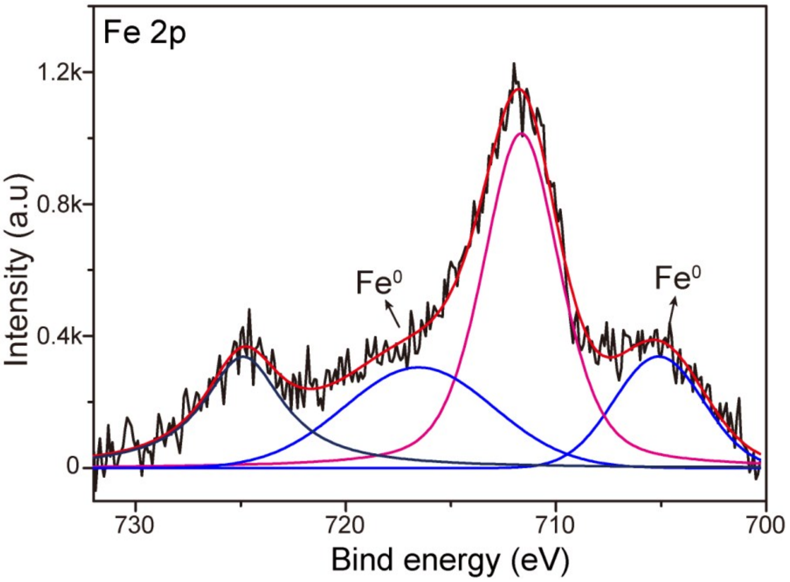

Fig. S6 Fe 2p core-level XPS spectra for n-Si/Ni/NiOOH/NiFe photoanode.

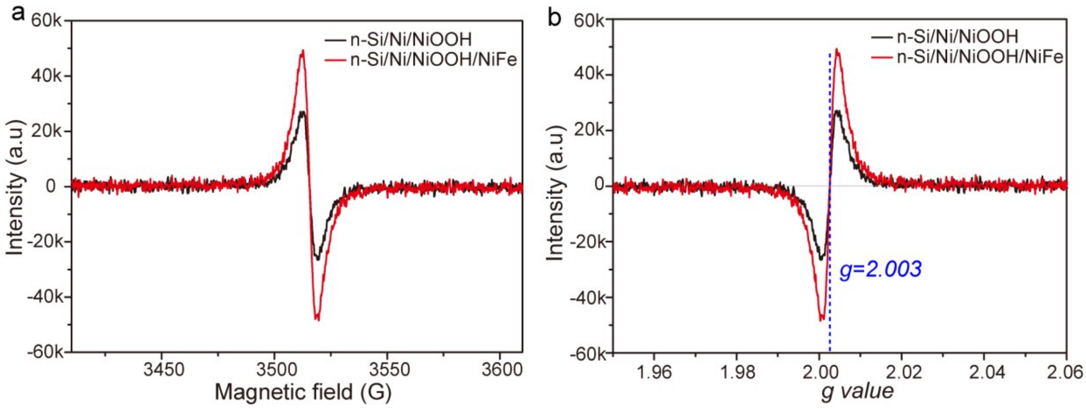

Fig. S7 EPR spectra of n-Si/Ni/NiOOH and n-Si/Ni/NiOOH/NiFe photoanodes.

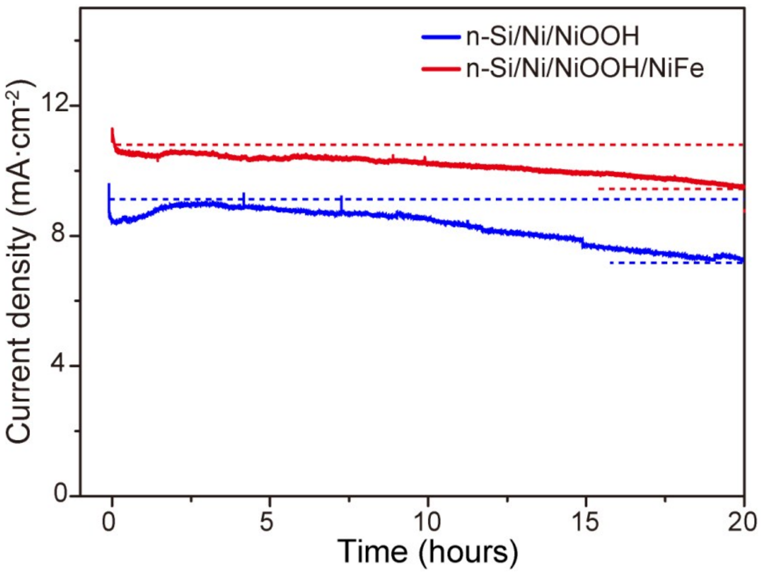

Fig. S8 The chronoamperometric curves of n-Si/Ni/NiOOH (blue curve) and n-Si/Ni/NiOOH/NiFe (red curve) photoanodes in 1.0 M K-borate electrolyte, respectively.

The electrochemical stability tests are performed in 1.0 M K-borate electrolyte at a constant external potential to obtain the initial current density around 10 mA·cm^{-2}. The chronoamperometric curves of n-Si/Ni/NiOOH and n-Si/Ni/NiOOH/NiFe photoanodes in **Fig. S8** demonstrate that the NiFe modification will enhance the stability of Si photoanode. The NiFe nanoparticles distributed on the bare Si surface can prevent Si contact with electrolyte.

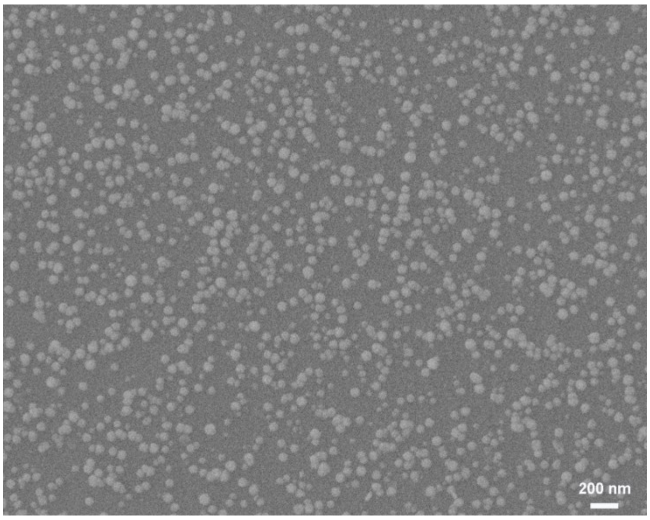

Fig. S9 SEM images of n-Si/Ni/NiOOH/NiFe photoanode after 20 hours stability operation.

The SEM image of the photoanode after long-term test have been provided as shown in **Fig. S9.** SEM images demonstrate that Si photoanodes can maintain its morphology after stability operation, further confirming the high stability of the Si photoanode.

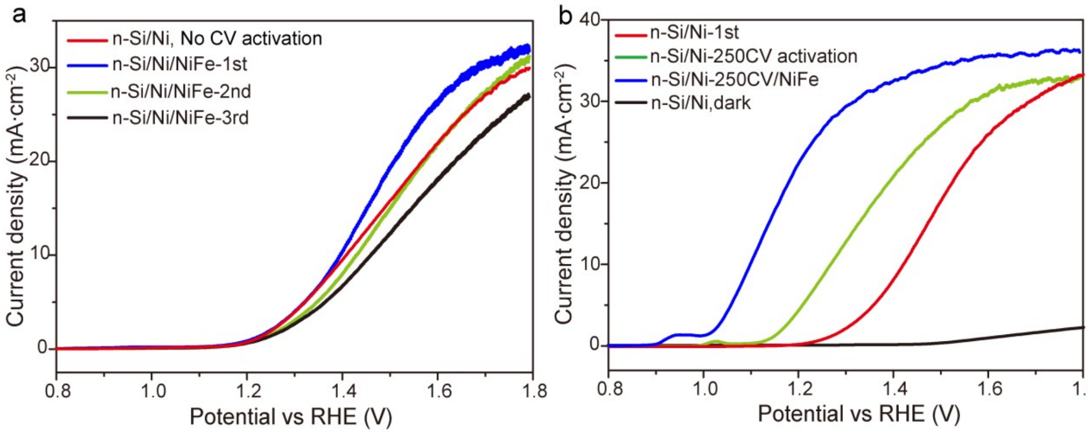

Fig. S10 (a) LSVs curves of n-Si/Ni/NiFe photoanodes without CV activation, which shows poor PEC activity and stability. **(b)** LSVs curves of n-Si/Ni/NiFe photoanodes with CV activation.

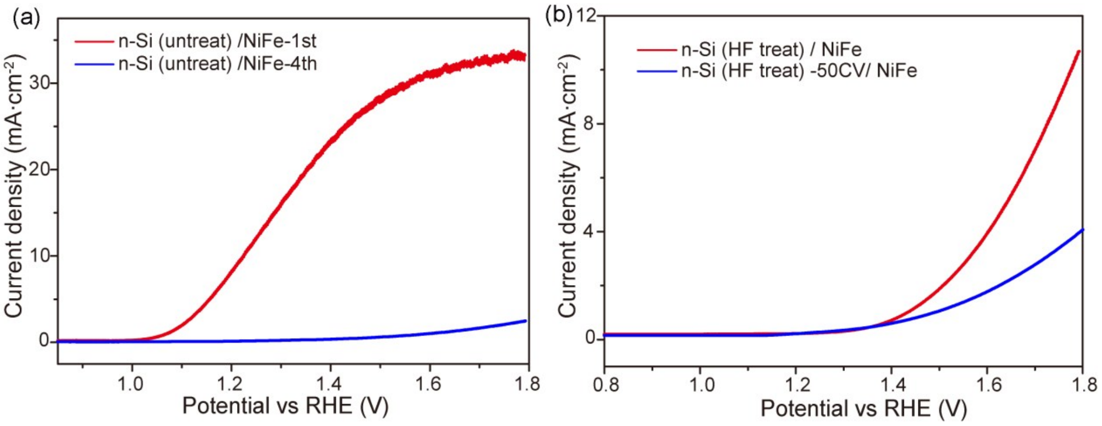

Fig. S11 (a) LSVs curves of n-Si/NiFe photoanodes with native SiO_x layer on untreated Si substrate. **(b)** LSVs curves of n-Si/NiFe photoanodes without native SiO_x layer on HF-treated Si substrate.

Different control experiments shown in **Fig. S10-S11** indicates that both the Ni NPs and the thin adventitious SiO_x layer play key roles in boosting OER performance Si photoanodes. Ni NPs core in this structure not only employed to protect Si photoanode, but also to extract and transfer charges from the depletion layer to the active surface layer. The interfacial SiO_x layer between Si semiconductor and NiFe NPs will reduce the Fermi-level pinning of Si substrate and also protect Si substrate from photocorrosion.

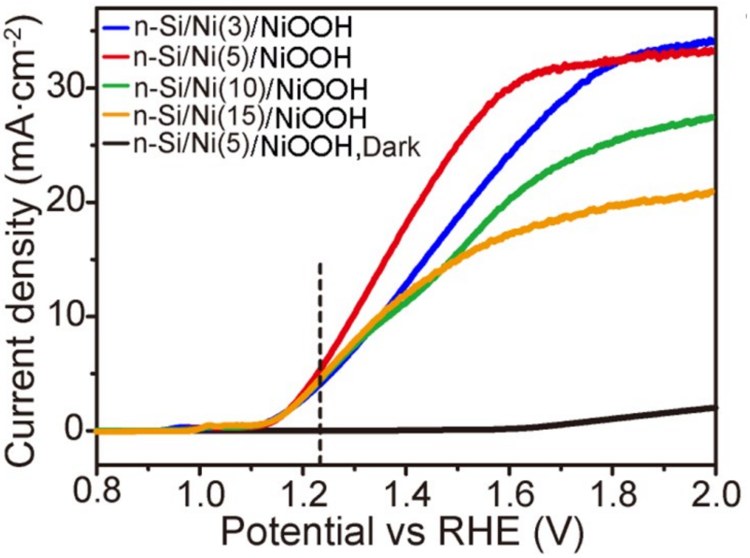

Fig. S12 LSVs curves of n-Si/Ni/NiOOH photoanodes in 1.0 M KOH electrolyte with various Ni deposition time: 3s, 5s, 10s, 15s.

To understand the n-Si/Ni interface and photoelectrode response, we measured the OER properties as a function of the Ni film thickness (**Fig. S12, ESI**). As the Ni electrodeposition time increases from 3 to 15 s, although the onset potential was almost independent with Ni thickness, there was a notable saturation photocurrent density decreased monotonically with increasing Ni thickness and can be explained by increased parasitic optical absorption associated with the opaque Ni particle.

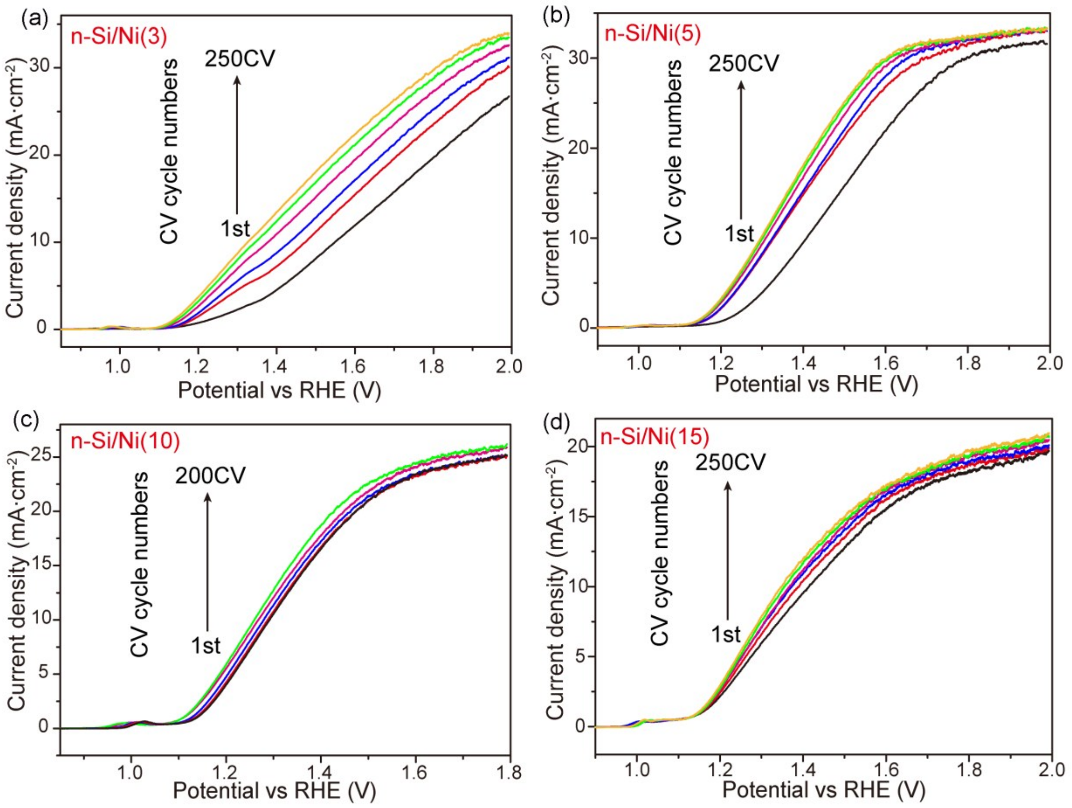

Fig. S13 The PEC performance of 250 consecutive CV cycles of n-Si/Ni photoanodes with various Ni nanoparticles electrodeposition time: **(a)** 3s, **(b)** 5s, **(c)** 10s, **(d)** 15s. The direction of the black arrow represents the gradual evolution of the PEC performance of the photoanodes.

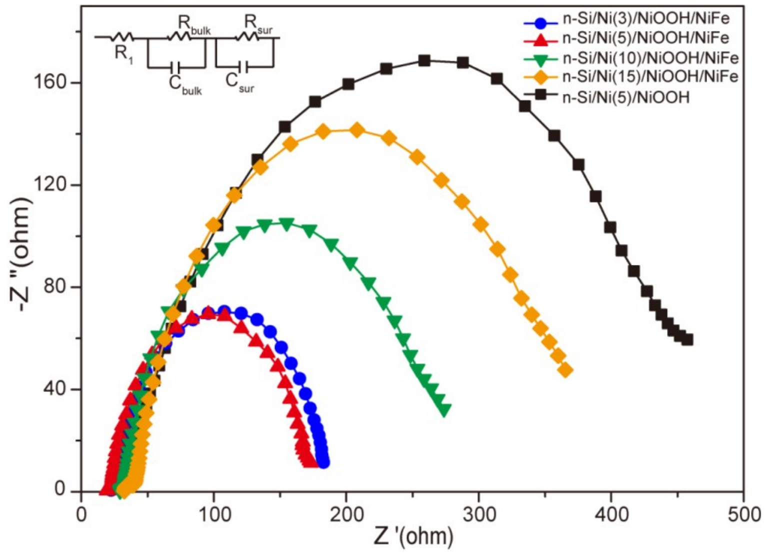

Fig. S14 Nyquist impedance plots (EIS) for n-Si/Ni//NiOOH/NiFe photoanodes with different Ni electrodeposition time.

Electrochemical impedance spectroscopy (EIS) measurements are conducted in 1 M KOM electrolyte. AC voltage is 5 mV amplitude with the frequency range from 0.1 Hz to 10000 Hz. The initial potential is around their corresponding onset potential. The fitted EIS spectra (**Fig. S14**) for all the photoanodes reveal two semicircles, which can be modeled to an equivalent circuit model (**Fig. S14** inset). The first and the second semicircle are ascribed to the bulk and surface charge transfer processes, respectively. The bulk charge transfers resistance (R_{bulk}) is derived from the underlying Si substrate under light illumination, while the second semicircle depicts the charge transfer resistance from the surface catalyst to the electrolyte.

The smaller charge transfer resistance (R_{ct}) of n-Si/Ni(5s)/NiOOH/NiFe photoanode, demonstrating the efficient separation of photo-generated electron-hole pairs and fast-interfacial charge transfer, which is according with excellent OER activity.